Development of Mach-Scale Swashplateless Rotor with Embedded Trailing-Edge Flaps

Jayant Sirohi [1], Keith Allen [2], Inderjit Chopra [3]
Alfred Gessow Rotorcraft Center,
University of Maryland, College Park,
MD, 20742, USA
[1] e-mail: sirohij@umd.edu
[2] e-mail: kmallen@umd.edu
[3] e-mail: chopra@umd.edu

Key words: Swashplateless, Trailing-edge flaps, Piezobender, Soft pitch link, Mach-Scale Rotor

Abstract: The goal of the present work is to experimentally validate the concept of swashplateless control using on-blade trailing-edge flaps in conjunction with soft pitch links. A Mach-scale composite rotor is constructed for hover and forward flight wind tunnel tests. Based on a previously conducted parametric study, design parameters such as flap location and size are chosen to minimize actuation requirements. The flaps are powered by piezobender actuators, which are optimized to meet the control requirements. Following extensive bench-top testing of the flap mechanism, the blades are mounted on a hover stand for rotating tests. While the rotor shows good structural integrity up to the design speed of 2400 RPM, initial tests indicate that the flaps are underpowered for Mach-scale operation. Therefore, tests are conducted up to speeds of 1200 RPM, with rotor speed, index angle, and blade torsional stiffness as test variables. Hover tests show that blade pitching can be achieved through the actuation of on-blade flaps, proving the concept of the swashplateless rotor. At a torsional frequency of 1.26/rev and with an index angle of 10°, the rotor demonstrated a change in steady and 1/rev blade pitch of ±1.5° and steady lift force of ±15%. However, several modifications must be made to the current trailing-edge flap actuators before further wind tunnel testing can be conducted.

INTRODUCTION

Helicopters typically employ a mechanical swashplate to achieve primary control and vehicle trim. The swashplate transmits control inputs from the fixed frame to the rotating frame by means of rigid pitch links. A typical swashplate assembly is bulky and mechanically complex. Consequently, the rotor hub contributes a significant fraction of the total parasite drag of the helicopter. In addition, a large amount of preventive maintenance and inspection of the swashplate assembly is necessary to ensure flight safety and reliability. Recently, there has been considerable interest in achieving primary flight control without the use of a swashplate. The main driving factors for a swashplateless rotor are the reduction in hub complexity and size, resulting in lower maintenance requirements as well as reduced parasite drag.

Several studies1–4 have shown that integrated trailing-edge flaps can satisfy the requirements for primary control, and thus replace the swashplate. Using a simplified aeroelastic model, Ormiston1 showed that trailing-edge flaps could potentially be used for primary control. The study also found that aerodynamic penalties from flap deflections could be reduced by indexing the rotor blades, and the blade fundamental torsional frequency must be lowered to between 1.5/rev and 2.5/rev for increased control authority. Shen and Chopra2 developed a comprehensive aeroelastic model of a swashplateless rotor to evaluate actuation requirements. The model was based on a five-bladed MD 900 bearingless rotor, which was modified by replacing the pitch link with a linear spring to lower the blade torsional frequency. The analysis determined that the rotor could be trimmed over a

complete range of advance ratios, and that flap actuation requirements could be reduced with blade pitch indexing. Following this work, Shen and Chopra conducted a numerical parametric study3 of the swashplateless rotor, and found index angle, root spring stiffness, and flap size and location to be key design parameters. The study also indicated that the swashplateless rotor has greater aeroelastic stability than a conventional rotor. Subsequently, Shen and Chopra4 evaluated the requirements of a trailing-edge flap for primary control of an ASI 496 helicopter during autorotation and maneuvering flight. They concluded that the required flap deflections and actuation power were moderate in these flight conditions, and that the chosen blade index needed to be a compromise among steady-level and maneuvering flights.

Although the analytical studies described above support the concept of trailing-edge flaps for primary control, there has been limited experimental work on this topic. Trailing-edge flaps actuated by piezobender actuators have been successfully employed for vibration control in Mach-scale5,6 and Froude scale7 wind tunnel tests. However, compared to vibration control, primary control necessitates the use of larger flaps, more powerful actuators, and lower blade torsional frequencies. The main challenge of trailing-edge flap actuation is the integration of actuators of sufficient power output within the blade geometry, while maintaining the structural, mass and aeroelastic constraints of the rotor blade.

Bao et. al.8 constructed a Mach-scale rotor with trailing-edge flaps actuated by piezobenders and performed some experiments on primary control authority. The main focus of this study was the parametric design of the rotor blade and trailing-edge flap to maximize the control authority. Due to complex kinematics of the actuators arising from the use of a twisted rotor blade with a large single flap, experiments were restricted to low rotational speeds.

The objective of the present study is to experimentally validate the primary control authority of on-blade trailing-edge flaps on a torsionally stiff rotor blade in conjunction with soft pitch links. The paper discusses the design, fabrication, and testing of a proof-of-concept Mach-scale swashplateless rotor with trailing-edge flaps actuated by piezobenders.

1. PRINCIPLE OF OPERATION

Trailing-edge flaps integrated in a rotor blade can be used to introduce pitching moments directly in the rotating frame, eliminating the need for a mechanical swashplate. However, to achieve a high level of control authority, the torsional frequency of the rotor blades should be around 1.5/rev – 2.5/rev1. The typical value of torsional frequency for a rotor blade is around 4/rev – 5/rev. The torsional frequency can be decreased by designing the blades to have a lower torsional stiffness. However, this can be a challenging problem in practice, especially for a scaled model. A low torsional frequency can also be achieved with torsionally stiff blades in conjunction with soft pitch links. In this manner, the structural integrity of the blade need not be compromised to achieve a lower effective torsional stiffness. Figure 1 shows the hub of a swashplateless rotor with a pitch spring attached between the torque tube and a support on the rotor shaft. This pitch spring acts in parallel with the torsional spring at the root of the blade and results in a lower control stiffness than in the case of a rigid pitch link. The blade is attached to the torque tube by an indexing splice, which imparts the appropriate index angle (pre-collective pitch) to the blade.

Deflecting the trailing-edge flaps creates a pitching moment on the rotor blade, resulting in a pitch change due to deformation of the pitch link spring. An upward flap deflection creates a nose-up moment that raises blade pitch and increases lift force, whereas a downward deflection has the

opposite effect. Steady up or down flap deflections produce collective pitch control, and properly phased sinusoidal flapping at the rotational frequency (1/rev) provides cyclic control.

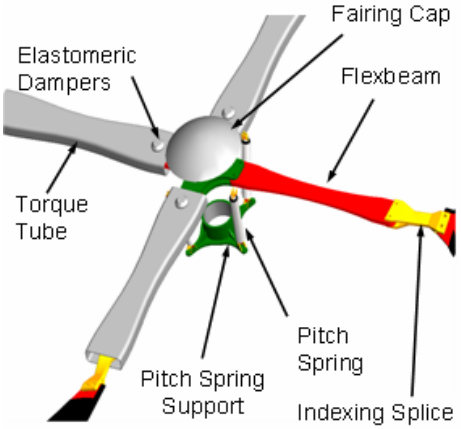

Figure 1. Swashplateless rotor hub construction

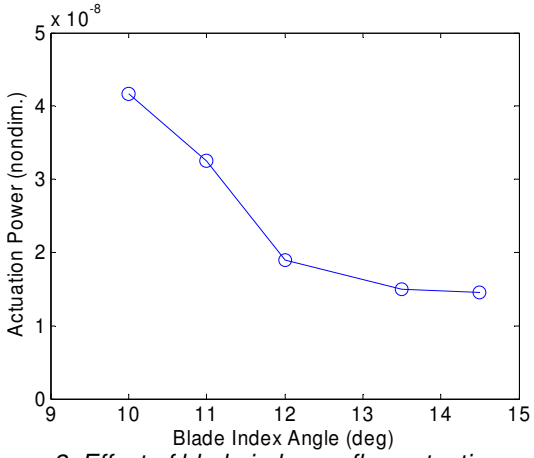

Figure 2. Effect of blade index on flap actuation power (flap length 0.2R, flap chord 0.15C, flap overhang 0.05C, CT /σ=0.08, μ=0.32)

2. SYSTEM DESIGN AND CONSTRUCTION

The present swashplateless rotor consists of two composite blades with integrated piezobender actuators and trailing-edge flaps. The model is designed for testing in the Glenn L. Martin wind tunnel at the University of Maryland, which imposes a constraint on the rotor diameter. In addition, an existing articulated rotor hub is used for all testing. The optimum geometry of the trailing-edge flaps is identified by a parametric study. Accordingly, the rotor blades have a length of 28 in (0.71 m), with a total diameter of 66 in (1.68 m). An operating speed of 2400 RPM is targeted to provide a tip Mach number of 0.65 during hover. To simplify construction, the blades feature a rectangular, untwisted planform with a uniform NACA0012 airfoil profile. The rotor blade consists of three distinct sub-assemblies: the load carrying structural assembly of the blade, the trailing-edge flap and actuator assembly and the soft pitch link. Each sub-assembly is carefully designed and tested separately on the bench-top to meet operational requirements.

2.1 Rotor Blade Parametric study

The small scale of the rotor necessitates the use of compact actuators to control the trailing-edge flap; therefore it is important to minimize the required actuation power. A parametric study8 using UMARC (University of Maryland Advanced Rotorcraft Code) was conducted on the baseline rotor to identify important design variables. Through this process, dimensions for flap size, location, and blade index angle were chosen to minimize actuation power and maximize control authority. By adjusting the pitch links to change the blade index angle, the blade pitch travel required for primary control is reduced. Thus, as blade index angle increases, the required flap deflection decreases and actuation power decreases, as shown in Figure 2.

Following the UMARC parametric study, a flap with a span of 28% radius and width 15% chord, centered at 75% radius is chosen. The control requirements for several different flight conditions are calculated for the selected rotor design, the maximum being a flap hinge-moment of 0.066 in-lb. (0.0075 N.m) and deflection of 5.5 degrees at an advance ratio of 0.32. The parameters of the rotor blade are shown in Table 1.

Table 1. Swashplateless rotor parameters

Number of blades	2
Rotor diameter	66 in (1.68 m)
Blade span	28 in (0.71 m)
Blade chord	3.15 in (0.08 m)
Airfoil profile	NACA 0012
Max. RPM	2400

2.2 Rotor blade construction

The baseline blade structure consists of a composite spar with an aluminum root insert, a leading edge foam cell with embedded leading edge weights, an aft foam cell, and a composite outer skin. The spar is the primary structural component, providing axial strength to sustain the centrifugal force, as well as attachment points for the flap mechanism to transfer the flap loads. The foam cells maintain the airfoil shape and the outer skin maintains the torsional rigidity. The flap on each rotor blade is split into two equal span flaps, and each flap is actuated by a separate piezobender. Therefore, each rotor blade contains two trailing-edge flap assemblies adjacent to each other. This design was adopted to minimize the effects of spanwise out-of-plane deformations of the flap. The entire rotor blade with the flap and piezobender assembly is designed and modeled in CATIA. A drawing of the rotor blade with dual trailing-edge flap assemblies is shown in Figure 3.

The spar is constructed by wrapping 8 strips of unidirectional graphite epoxy (AS4/3501) prepreg around an aluminum root insert. An additional strap of graphite epoxy unidirectional prepreg is wrapped perpendicular to the spar, around the tip of the root insert to prevent delamination due to centrifugal forces at the spar/root interface. Three holes drilled into the root insert provide attachment points between the blade and the blade grip on the existing rotor hub. The assembled spar is then cured in a compression mold. The resulting product is a solid composite beam of 0.33 in (8.4 mm) height and 0.12 in (3.05 mm) thickness, with an embedded aluminum root insert (Figure 4). With a predicted blade mass of 300 grams placed at the tip, the spar experiences a maximum load of 16,500 N. A tensile test of a finished spar using an MTS material test machine confirmed its structural integrity up to a load of 18,000 N, at which point the single supporting bolt pulled through the aluminum insert. With the added support of the skin and two additional mounting bolts, the finished blades support the worst-case load with an adequate safety factor.

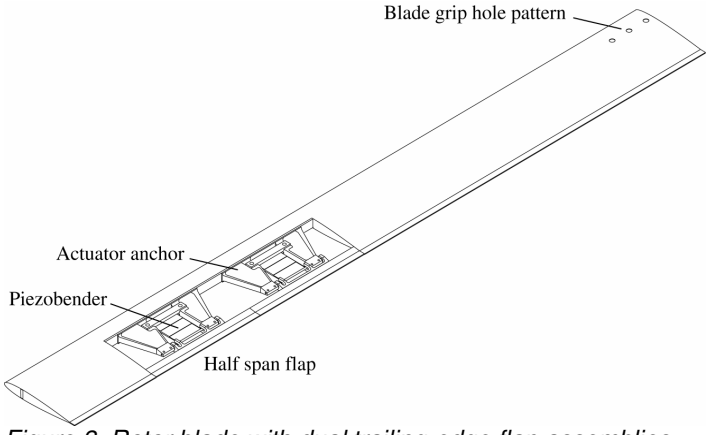

Figure 3. Rotor blade with dual trailing-edge flap assemblies

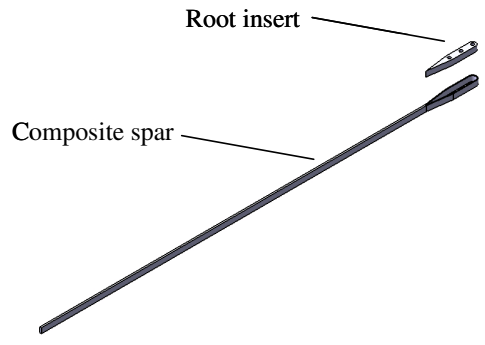

Figure 4. Composite blade spar with aluminum root insert

After constructing the spar, the remainder of the blade is assembled. Low density Rohacell foam is cured in a compression mold to impart the airfoil shape and is subsequently machined into the appropriate shapes for the forward and aft foam cells. A pocket is machined into the aft foam cell to accept the flap and piezobender assembly. Tungsten leading edge weights are embedded into the leading edge foam cell and fixed in place with film adhesive, and power/sensor wires are embedded into the aft foam cell. Next, the spar and both foam sections are wrapped in film adhesive and pressed tightly together. The assembly is then wrapped in two plies of 0/90 woven graphite epoxy cloth, compressed in a mold, and cured. Next, the outer skin and foam aft of the spar are removed at the location of the flap. Finally, the trailing-edge flap assembly is bonded to the spar and covered using the sections of outer skin removed earlier. The steps involved in the assembly of the rotor blade are shown in Figure 5.

2.3 Trailing-edge flap assembly

The trailing-edge flap assembly consists of three parts: the actuator anchor, the trailing-edge flap and the piezobender assembly. The assembly is shown in Figure 6. During assembly, all parts are held within a jig and bonded together to ensure precise and uniform construction of each flap.

2.3.1 Actuator anchor

The actuator anchor must provide a rigid support for the hinge on which the flap is mounted, as well as for a pair of clamps to which the piezobender is bonded. Maximizing the stiffness of this support will result in the most efficient transfer of deflection from the piezobender to the flap. To provide the necessary stiffness with minimal weight, the anchor consists of two wide, tapered I-beams machined from a single piece of aluminum. The anchor is designed for a maximum deflection of 0.0014 in (0.035 mm) at a rotational speed of 2400 RPM while supporting its own inertial load, as well as the loads of the piezobender and flap. The shaft on which the flap rotates is held in place at the ends of the anchor by setscrews, and the piezobender clamps are held on to the anchor by means of two pins. The deformation of the anchor calculated using a commercial finite element analysis package is shown in Figure 7.

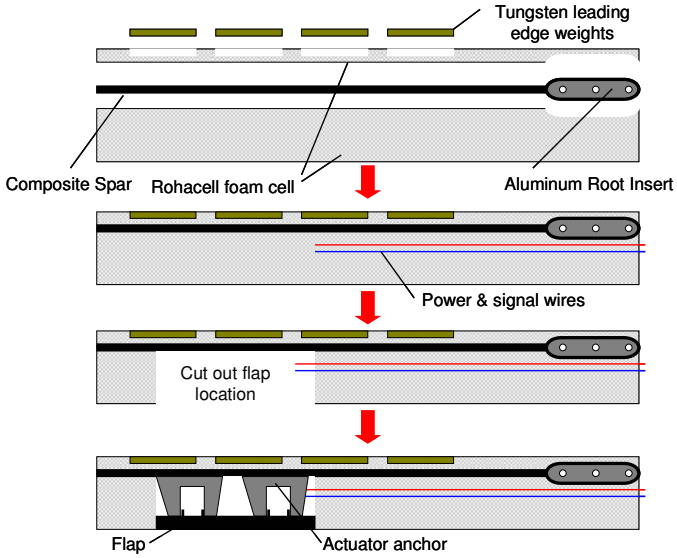

Figure 5. Fabrication process for blade with integrated flap

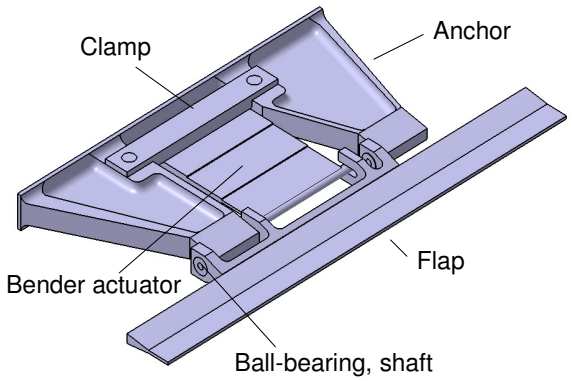

Figure 6. Trailing-edge flap actuator assembly

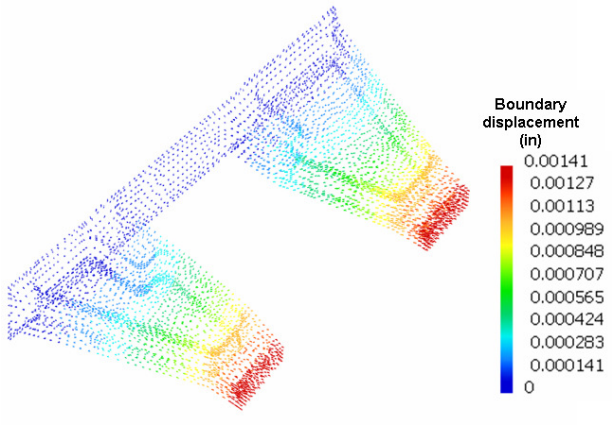

Figure 7. Anchor deflection under simulated loading

2.3.2 Flap construction

The trailing-edge flap is constructed by cutting out the trailing-edge of the cured rotor blade. Each flap is bonded to an aluminum support that also houses miniature radial ball bearings. The flap hinge is formed by these bearings assembled on the shaft attached to the ends of the anchor. The motion of the piezobender is transmitted to the flap through a cusp machined into the flap support. The flap bonded to the aluminum support is shown in Figure 8.

2.3.3 Piezobender assembly

The limited volume and weight constraints of the rotor blades present a unique challenge regarding the design of the flap mechanism. The actuator and flap supports must provide sufficient control authority and structural strength for high speed rotation, while fitting within the 0.34 inch thick airfoil and adding minimal weight. Piezoelectric bender actuators are chosen to meet these design constraints due to their compactness and energy efficiency.

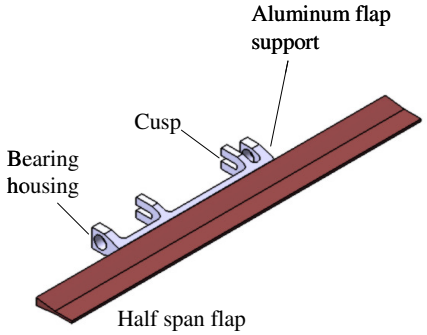

Figure 8. Half span flap and flap support

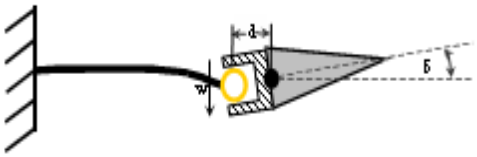

Figure 9. Schematic of piezobender actuation

The actuators are constructed in-house using commercially available PZT-5H piezoelectric sheets. Figure 9 shows a simple schematic of the flap mechanism. The piezobender is cantilevered at the root end, and is mated to the trailing-edge flap by a pin-cusp assembly. An offset between the pin and the flap hinge results in an amplification of the tip deflection of the piezobender and an angular deflection of the trailing-edge flap. The optimum piezobender geometry is determined by a parametric study using a finite element model, which treats the piezobender as an Euler-Bernoulli beam with non-linear induced strain actuation. The model was validated by experiments on two

different piezobenders, and was subsequently used to investigate the effects of length, thickness taper, number of layers, rotational speed, and hinge-offset on piezobender performance. The design variables of length, thickness taper, and number of layers determine the balance between stroke and force output. Hinge-offset and total piezobender length are constrained by fabrication tolerances and blade dimensions. Flap deflection angle δ and hinge moment Mh can be directly related to the bender tip displacement w and actuation force F, as a function of the hinge-offset d. Using a small-angle assumption,

$$F = \frac{M_h}{d} = \frac{M_h \delta}{w} \quad (1)$$

Hence, a plot of the actuator force and stroke is generated for different piezobender geometries and is compared to the control requirements (Figure 10). From these results, an optimal bender design is chosen, with dimensions listed in Table 2.

Table 2. Piezobender configuration

Number of PZT layers	8
Cantilevered length	1.08 in (27.4 mm)
Width	1.00 in (25.4 mm)
Shim thickness	2 mil (0.051 mm)
Thickness taper pattern	1.08/1.08/0.58/0.33 in (27.4/27.4/14.7/8.4 mm)
Total thickness	85 mil (0.22 mm)
Weight	10.5 grams

Table 3. Weight breakdown of rotor blade with trailing-edge flap

Component	Mass (gm)
Blade	101
Main spar	27
Anchor (each)	12
Actuator clamp (each)	2
Piezobender (each)	9
Flap mount (each)	2
Flap (each)	3
Leading edge mass	89
TOTAL	279

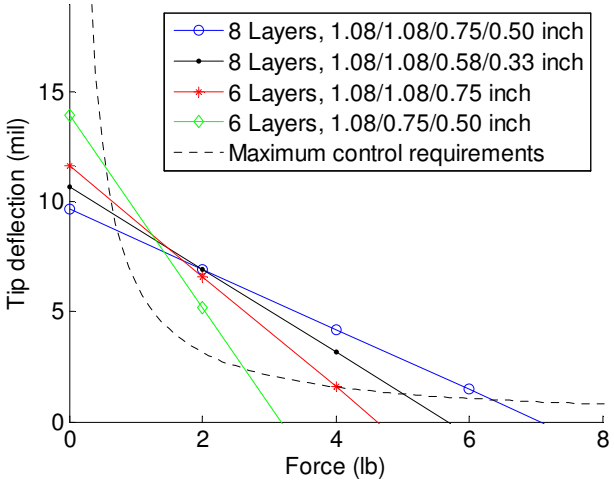

Figure 10. Parametric study of piezobender configuration

Each piezobender consists of eight piezoelectric sheets bonded to a central brass shim (Figure 11). The sheets on opposite sides of the shim are excited to produce opposing strain, creating a pure bending deformation. Note that the dots in the figure represent the positive electrode of the piezoelectric sheets. To take advantage of the high piezoelectric capability of the PZT sheet in the polarization direction, the actuator is powered using a 3:1 AC bias. The cantilevered condition at the root is implemented by bonding the piezobender to two aluminum clamps which are attached to the actuator anchor by means of tight fitting pins (Figure 12). The pin at the tip of the piezobender is a steel shaft bonded on by two plies of fiberglass, and slides in the cusp machined into the flap support.

The weight breakdown of all the components of the final assembled rotor blade is given in Table 3.

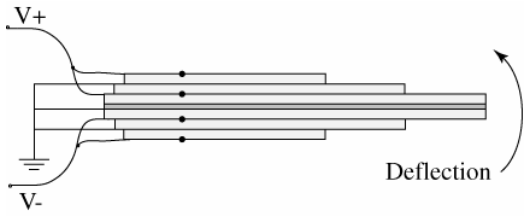

Figure 11. Schematic of piezobender layup

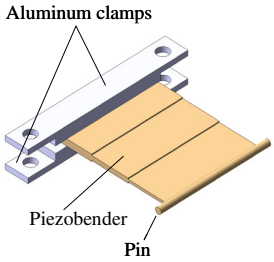

Figure 12. Aluminum clamps and pin bonded to piezobender

2.4 Soft Pitch Link assembly

Each soft pitch link consists of a low-friction linear slide with precision tension springs attached to each end (Figure 13). A linear potentiometer mounted to the slide is calibrated to provide blade pitch measurements. The pitch link is attached in place of the conventional rigid pitch link, between the blade-pitch horn and rotating swashplate. This design allows for low-friction compression or extension of the pitch link when the blade is subjected to a pitching moment, while the linear slide sustains all the off-axis loads without seizing. Furthermore, the springs can easily be changed to achieve the desired torsion frequency. An assembled pitch link is shown in Figure 14.

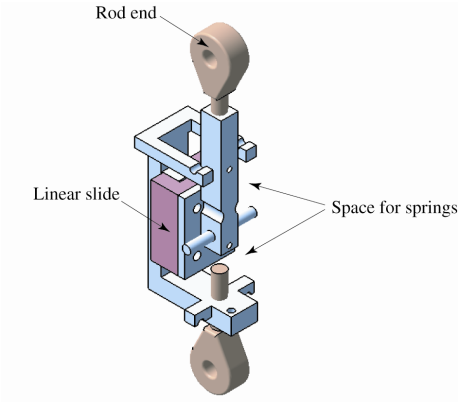

Figure 13. Schematic of soft pitch link

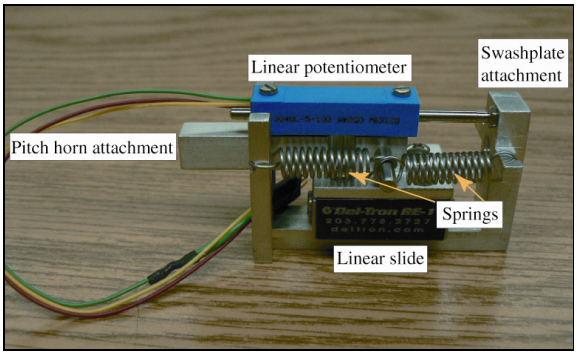

Figure 14 Assembled spring loaded pitch link

2.5 Hover stand installation

The swashplateless rotor is tested in hover on a rotor test stand at the University of Maryland (Figure 15). A fixed frame balance is used to measure hub forces and moments. Flap deflections are measured using Hall Effect sensors on the blades, and blade pitch angles are determined through linear potentiometers mounted to the pitch links. Data is transferred between the rotating frame and fixed frame via a 64-wire slip-ring mated to the rotor shaft below the drive pulley. A 16-wire power slip-ring is used to supply power to the piezobenders. A close-up of the trailing-edge flaps on the rotor blade is shown in Figure 16. The existing swashplate is used to input blade index angles by means of an appropriate collective pitch.

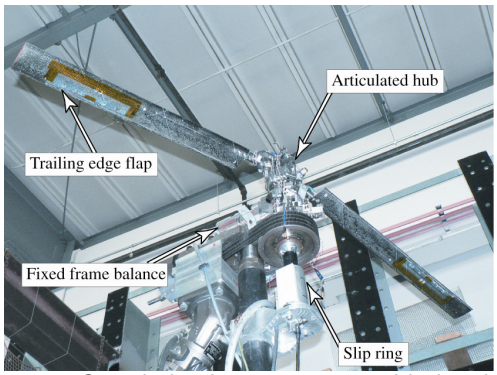

Figure 15. Swashplateless rotor assembled on hover stand

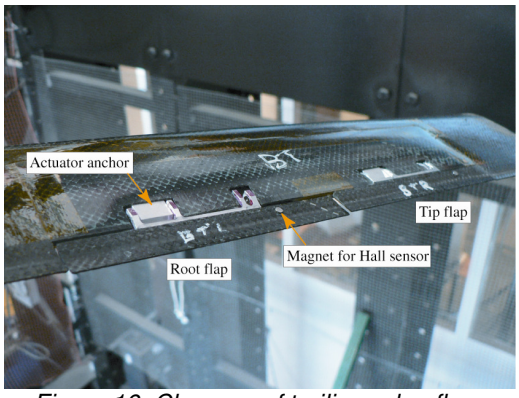

Figure 16. Close-up of trailing-edge flaps

3. EXPERIMENTAL RESULTS

The piezobenders were tested on the benchtop to measure their force and stroke characteristics. The blades were then assembled, calibrated, mounted on the rotor stand and systematically tested at different rotational speeds.

3.1 Benchtop tests

To verify the performance of the piezobenders, two were randomly selected from a set of eight finished actuators for static stiffness and actuation testing. The piezobenders were cantilevered at the root with a free length of 1.08 in (27.4 mm), and a laser displacement sensor was used to measure tip deflections. For the static stiffness test, loads up to 1.75 lb. (7.78 N) were applied to the tip of the piezobender. The resulting deflections, plotted in Figure 16, were close to the predicted values and indicated uniform mechanical properties of the two piezobenders. Tip deflections of both piezobenders were also measured under excitation voltages ranging from 25 to 120 volts with a 3:1 AC bias. The actuators were excited at a frequency of 1 Hz to measure quasi-steady behavior. The test results in Figure 17 show that both benders exhibited linear deflection-voltage characteristics up to the peak deflection of 13 mils (0.33 mm) at 120 volts.

Following the actuator benchtop tests, the flap assemblies were mounted within the rotor blades. Further actuation tests were conducted to verify flap performance and to calibrate the Hall Effect sensors used to measure flap angle. The four flaps showed uniform characteristics, with maximum deflections ranging from 12.3° to 13.6°. Hall Effect sensor voltages were linear over the full range of flap angles.

3.2 Hover tests

3.2.1 Rigid Pitch Link Tests

The blades were first tested with rigid pitch links to verify blade structural integrity and to evaluate flap performance under aerodynamic loading. The swashplate was leveled using an inclinometer prior to testing, and the rotor was subsequently checked to ensure that the blades were properly tracked. Blade pitch index was set to 5° for all rigid pitch link tests.

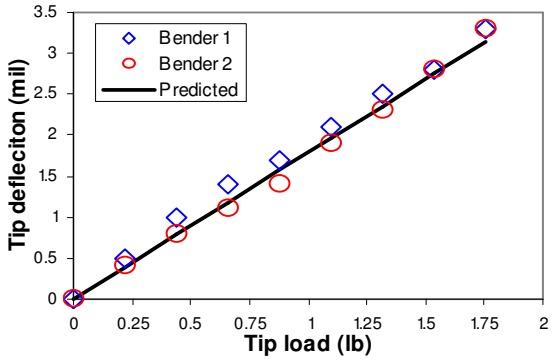

Figure 17. Piezobender steady force-deflection measurements

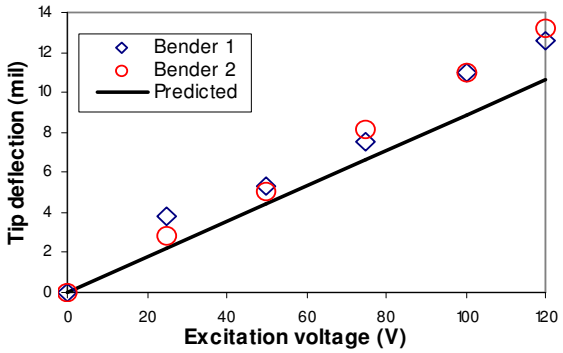

Figure 18. Piezobender tip deflection, 1 Hz excitation

The flaps were actuated with a DC voltage to input steady upward deflections at various rotor speeds. The resulting flap deflections are shown in Figure 18. The deflections for the root flap on blade A could not be measured due to a malfunctioning slip ring channel. As rotational speed increased, a steep drop in flap deflections was observed. Although this trend is expected due to increasing aerodynamic forces, flap deflections dropped to the target value of 5.5° by 900 RPM, and continued to decrease to less than 2° at 1500 RPM. It was concluded that this rapid decline in flap performance was due to an unexpectedly high hinge moment.

Based on the initial flap sizing study, the flaps were predicted to experience a maximum hinge moment of 0.066 in-lb (0.0075 N.m). at a rotor speed of 2400 RPM, advance ratio of 0.32, and $C_T/\sigma = 0.08$. Using the actuator stiffness values experimentally determined during bench-top testing, the actual hinge moment on the flaps can be calculated as

$$M_h = K_{actuator}(\theta_{free} - \theta) \qquad (2)$$

where M_h is the hinge moment, $K_{actuator}$ is the actuator stiffness, and θ_{free} and θ are the free and measured flap deflections respectively. The variation of measured hinge moment with rotor speed shown in Figure 19 indicates that aerodynamic loads reach the design value of 0.066 in-lb (0.0075 N.m) at less than 1000 RPM. Extrapolating these results to the original design speed of 2400 RPM yields a new predicted hinge moment of 0.215 in-lb (0.0244 N.m). Consequently, it was determined that the present piezobenders are not suitable for Mach-scale operation, and subsequent testing was limited to a maximum rotational speed of 1200 RPM.

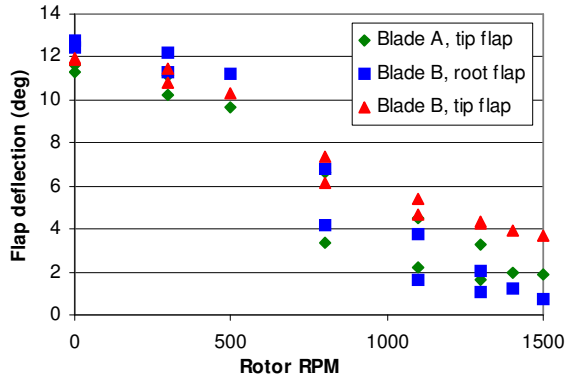

Figure 19. Effect of rotor speed on measured steady flap deflection

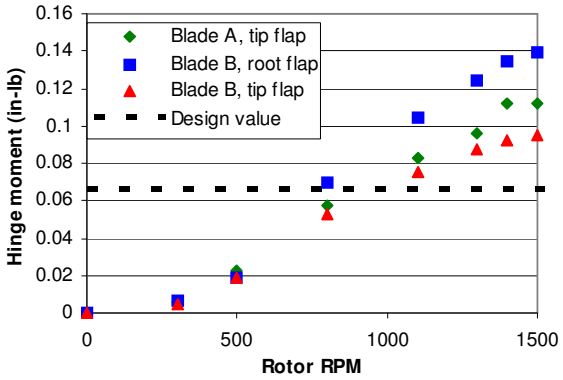

Figure 20. Measured steady trailing-edge flap hinge moments

3.2.2 Soft Pitch Link Tests

Further testing was performed at 900 RPM and 1200 RPM by replacing the rigid pitch links with the spring-loaded soft pitch links. Four sets of pitch springs, with stiffnesses ranging from 7 lb/in. to 32 lb/in. were tested. These resulted in effective blade torsional frequencies as shown in Table 4. The third test variable was blade index angle, which was set at either 10° or 15°.

For each test configuration, data were recorded for four cases: baseline (no flap movement), steady flaps up, steady flaps down, and 1/rev sinusoidal actuation. The data collected includes blade pitch, flap deflection angles, rotor lift force, and rotor total moment. Stable operation of the blade was observed under all test conditions.

Table 4. Blade rotating torsional frequencies with spring loaded pitch links

Pitch Spring Stiffness	7 lb/in (1227 N/m)	12 lb/in (2103 N/m)	16 lb/in (2804 N/m)	32 lb/in (5608 N/m)
900 RPM	1.26/rev	1.29/rev	1.4/rev	1.63/rev
1200 RPM	1.16/rev	1.17/rev	1.24/rev	1.39/rev

3.2.2.1 Swashplateless collective pitch input

A steady positive or negative deflection of the flap was achieved by actuating the piezobender with a DC voltage. This was equivalent to a collective pitch input to the rotor. In all test cases, steady deflection of the flaps produced the expected result: deflecting the flaps up caused the blades to pitch up and increased lift force, and vice versa.

Figure 20 and Figure 21 show the measured lift force and blade pitch for the full range of pitch spring stiffnesses at 900 RPM and 10° index angle. Flap effectiveness, which can be defined as the change in lift force or blade pitch from baseline, is seen to increase with decreasing spring stiffness, which corresponds to a lower torsional frequency. For example, deflecting the flaps upward increases blade pitch by 1.39° and lift force by 1.42 lb. when using 7 lb/in. pitch springs, but only increases pitch by 0.76° and lift by 0.37 lb. with the 32 lb/in. springs installed. Hover tests with different rotor speed and index angle configurations indicated a similar relationship between pitch spring stiffness and flap effectiveness. Note that the 1/rev flap excitation does not produce any noticeable change in steady lift force and steady blade pitch compared to the baseline values.

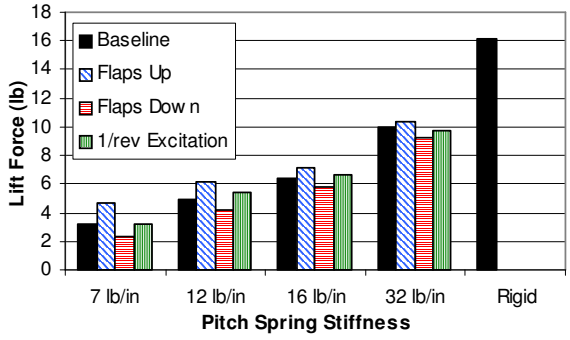

Figure 21. Measured steady lift forces, 900 RPM, 10° index angle

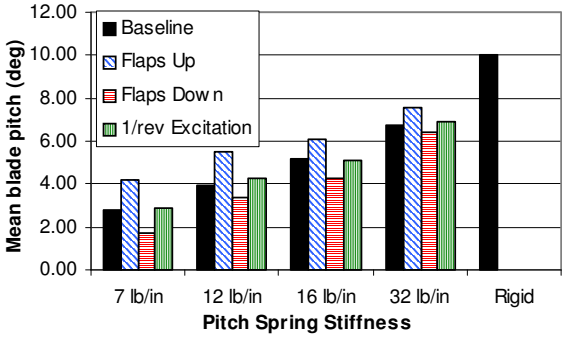

Figure 22. Measured steady blade pitch, 900 RPM, 10° index angle

An additional effect of introducing an index angle is a decrease in blade pitch with increasing rotational speed. This effect occurs due to a nose-down propeller moment that acts on the blade and

deforms the soft pitch link, resulting in a decrease in blade pitch. To minimize this effect, the chordwise position of the blade center of gravity should be as close to the feathering axis as possible while maintaining a sufficient margin of blade stability. The effect is more pronounced in the case of softer pitch springs, and can be seen as an increase in baseline mean blade pitch with increasing pitch spring stiffness in Figure 22. For a rigid pitch link, the baseline blade pitch should be the same as the blade index angle.

The baseline blade pitch is shown as a function of rotor RPM in Figure 23 for different values of spring stiffness and index angle. It can be seen that the magnitude of the pitch change is significantly larger at a higher index angle. At a 10° index angle, blade pitch decreases 1.0°-1.5° from 900 RPM to 1200 RPM, whereas the same speed change results in a pitch decrease of 1.75°-2.25° with a 15° index angle. Note that although baseline blade pitch declines from 900 RPM to 1200 RPM, measured lift forces are similar at both speeds, as the pitch decrease is offset by increased dynamic pressure.

As observed previously with the rigid pitch links, flap deflections decreased as rotor speed increased, approaching from between 4° and 4.5° at 900 RPM to between 1.75° and 2.5° at 1200 RPM. In spite of this, flap performance in terms of change in blade pitch and lift force, remained fairly constant between both rotor speeds, due to the increased dynamic pressure at 1200 RPM. Figure 24 shows the changes in normal force produced by deflecting the flaps up and down at both 900 RPM and 1200 RPM, for two sets of pitch link springs. With the softer springs, deflecting the flaps induces lift changes from -0.63 lb (2.8 N) (flaps down) to +1.19 lb (5.29 N) (flaps up) at 900 RPM, and from -0.92 lb (4.09 N) to +1.19 lb (5.29 N) at 1200 RPM. These force changes correspond to respective overall lift percentage changes of -7.1% to +13.4% at 900 RPM and -9.6% to +12.3% at 1200 RPM.

Figure 25 and Figure 26 show the measured blade pitch angles and lift forces as a function of index angle and rotor speed, using 16 lb/in. pitch springs. At 900 RPM, flap deflections produce lift changes ranging from -0.64 lb (2.85 N) (flaps down) to +0.66 lb (2.93 N) (flaps up) with an index of 10°. Increasing the index angle to 15° improves flap effectiveness by almost 50%, as lift force changes range from -0.87 lb (3.87 N) to +0.93 lb (4.14 N).

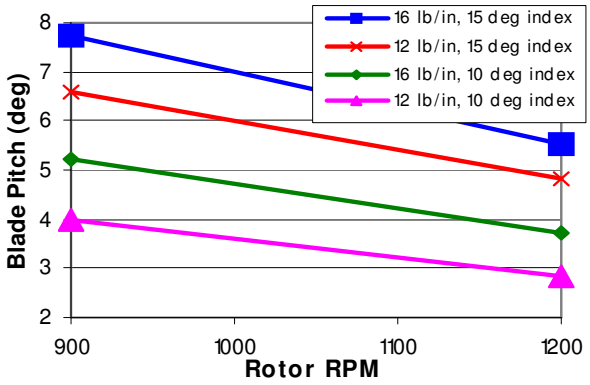

Figure 23. Effect of rotor speed, pitch stiffness and blade index angle on baseline blade pitch

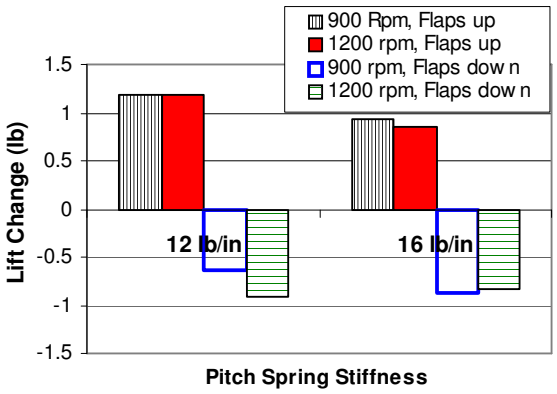

Figure 24. Change in steady lift force at 10° index, at different rotor speed and pitch stiffness

The performance benefits of a high index angle are even more pronounced at higher rotor speeds. At 1200 RPM and 10° index, deflecting the flaps produces lift changes from +0.07 (0.3 N) to +0.86 lb (3.83 N). With an index angle of 15°, the flaps are capable of lift changes from -0.83 lb (3.69 N)

to +0.86 lb (3.83 N). Note that the initial parametric design study indicated that the flaps would be most effective for swashplateless control at a blade index angle of 14.5° (Figure 2). Increasing baseline blade index angle from 10° to 15° was observed to produce an improvement in flap effectiveness of up to 50%, validating the conclusion of the parametric study.

3.2.2.2 Swashplateless cyclic pitch input

Swashplateless cyclic pitch input was accomplished by actuating the flaps sinusoidally at a frequency of 1/rev. If the excitation of each blade is properly phased, then the resulting oscillatory blade pitching will produce cyclic pitch or roll moments. During hover testing, very high baseline rotor pitch moments were observed. This was attributed to differences in the equilibrium position of the spring loaded pitch links, leading to a steady cyclic input. Furthermore, as the present test setup does not have the ability to synchronize flap actuation to the rotor azimuthal position, pitch and roll moments cannot be measured independently. For these reasons, the cyclic control authority was evaluated in terms of induced 1/rev blade pitch amplitude.

Using the 7 lb/in. pitch springs, a 1/rev flap input produced sinusoidal blade pitching with an amplitude of 1.50°, as shown in Figure 27. As expected, the flap effectiveness increased with decreasing torsional frequency. The amplitude difference between blades A and B is due to slight dissimilarities during fabrication.

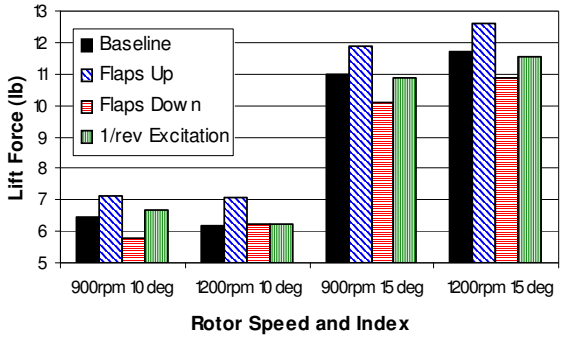

Figure 25. Measured steady lift force, 16 lb/in. pitch springs

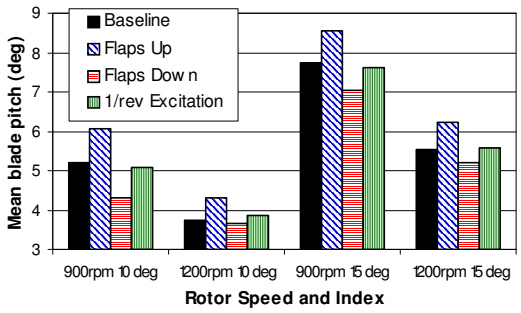

Figure 26. Measured steady blade pitch, 16 lb/in. pitch springs

With the 32 lb/in. springs installed, 1/rev actuation could only induce blade pitching of 0.36° amplitude. Increasing rotor speed from 900 RPM to 1200 RPM severely reduced flap effectiveness due to the decreased trailing-edge flap deflection arising from increased hinge moments. The maximum pitching amplitude observed at 1200 RPM is only 0.28°, which occurred using 12 lb/in. pitch springs and a 10° index angle. Conversely, the minimum amplitude observed at 900 RPM is 0.36°. Altering the index angle appeared to have a minor effect on induced 1/rev pitching amplitudes.

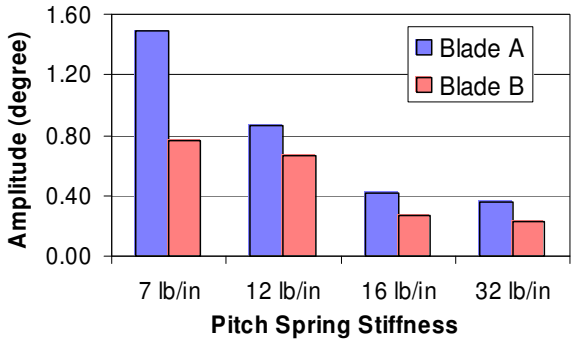

Figure 27. Pitch amplitude for 1/rev flap input, 900 RPM, 10° index angle

4. SUMMARY AND CONCLUSIONS

The concept of a swashplateless rotor incorporating integrated trailing-edge flaps in conjunction with soft pitch links was experimentally investigated through the design, fabrication, and hover testing of a Mach-scale rotor. A two bladed rotor of 66 in (1.68 m) diameter and 3.15 in (0.08 m) chord, with an integrated flap having a span of 28% radius and a width of 15% chord was designed and fabricated. The trailing-edge flaps were actuated by piezobenders. A minimum effective torsional frequency of 1.16/rev was achieved with the soft pitch links. The weight of the final blade assembly was 279 gm, and the rotor was successfully tested for structural integrity and blade stability up to 2400 RPM. Due to an underprediction of trailing-edge flap hinge moments, hover tests were restricted to a maximum rotor speed of 1200 RPM, which was half of the intended Mach-scale speed. A trailing-edge flap deflection of 12° was achieved in the non-rotating condition, which decreased to 2° at 1500 RPM.

Proof-of-concept of the swashplateless rotor system was established through steady and 1/rev actuation of the trailing-edge flaps and measurement of resulting blade pitch angles and lift forces in hover. A steady upward flap deflection was observed to result in a nose-up blade pitch and a corresponding increase in lift, and vice versa. For the torsional frequency of 1.26/rev and with an index angle of 10°, the rotor demonstrated a change in steady blade pitch of ±1.5° and steady lift force of ±15%. During the testing, it was observed that propeller moments resulted in a significant decrease in flap deflection with RPM. For example, at a torsional frequency of 1.24/rev, the blade index angle set at 15° decreased to 5.5° at 1200 RPM. In addition, it was observed that increasing the blade index angle from 10° to 15° resulted in an increase in flap effectiveness of up to 50%. For a 1/rev trailing-edge flap actuation under the same conditions, the rotor demonstrated a blade pitch amplitude of ±1.5°.

Though the present rotor with piezoceramic actuators successfully demonstrated swashplateless pitching, alternative flap actuation mechanisms are being explored. The low stiffness of multilayer piezobenders is insufficient for flap control at Mach-scale speeds. Accurate modeling and prediction of trailing-edge flap hinge moments is key to the future design and development of trailing-edge flap actuators as well as the overall swashplateless rotor system. Alternate actuator technologies, such as small (6-10mm diameter) brushless motors or macro fiber composite (MFC) actuators may result in more powerful actuators and satisfy the power requirements of higher rotor speeds. Following a comparative evaluation of several different actuators, a new generation of swashplateless blades will be constructed for high-speed hover tests and forward flight wind tunnel tests.

ACKNOWLEDGMENTS

This research was funded by the Aviation Applied Technology Directorate under contract number W911W6-05-C-0007 with Dr. Tin-Chee Wong and Dr. John Berry as technical points of contact. The authors would like to thank Techno-Sciences, Inc for their support.

REFERENCES

[1] R. A. Ormiston, "*Aeroelastic Considerations for Rotorcraft Primary Control with On-Blade Elevons*", Proceedings of the American Helicopter Society 57th Annual Forum, Washington DC, June 9-11, 2001.

[2] J. Shen, and I. Chopra, "Swashplateless Helicopter Rotor with Trailing-Edge Flaps", *Journal of Aircraft*, Vol.41, No.2, Mar.-Apr. 2001, pp.208-214.

[3] J. Shen, and I. Chopra, "A Parametric Design Study for a Swashplateless Helicopter Rotor with Trailing-Edge Flaps", *Journal of the American Helicopter Society*, Vol. 49, No. 1, Jan., 2004, pp. 43-53.

[4] J. Shen, and I. Chopra, "*Actuation Requirements of Swashplateless Trailing-Edge Flap Helicopter Rotor in Maneuvering and Autorotation Flights*", Proceedings of the American Helicopter Society 60th Annual Forum, Baltimore, MD, June 7-10, 2004.

[5] N. A. Koratkar, and I. Chopra, "Wind Tunnel Testing of a Smart Rotor Model with Trailing-Edge Flaps", *Journal of the American Helicopter Society*, Vol.47, No.4, October 2002, pp.263-272.

[6] B. Roget, and I. Chopra, "*Development and Testing of an Individual Blade Control Algorithm for Vibration Reduction of a Dissimilar Rotor*", Proceedings of the American Helicopter Society 60th Annual Forum, Baltimore, MD, June 7-10, 2004.

[7] M. V. Fulton, and R. A. Ormiston, "*Small-Scale Rotor Experiments with On-Blade Elevons to Reduce Blade Vibratory Loads in Forward Flight*", Proceedings of the American Helicopter Society 54th Annual Forum, Washington, DC, May 20-22, 1998.

[8] J. Bao, K. Allen, and I. Chopra, "*Design and Test of a Mach-Scale Swashplateless Rotor Using Smart Trailing-edge Flaps*", Proceedings of the American Helicopter Society 62nd Annual Forum, Phoenix, AZ, May 9-11, 2006.